Corrosion Science 230 (2024) 111877

Contents lists available at ScienceDirect

Corrosion Science

journal homepage: www.elsevier.com/locate/corsci

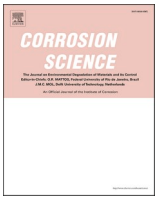

Enhanced steam oxidation resistance of uranium nitride nuclear fuel pellets

Jennifer H. Stansby [a,b,*], Yulia Mishchenko [c], Sobhan Patnaik [c,d], Vanessa K. Peterson [e], Christopher Baldwin [e], Patrick A. Burr [a,b], Denise Adorno Lopes [c,f,g], Edward G. Obbard [a,b]

[a] School of Mechanical and Manufacturing Engineering, UNSW, Sydney, NSW 2033, Australia
[b] UNSW Nuclear Innovation Centre
[c] Department of Physics, Nuclear Engineering Division KTH Royal Institute of Technology, Alba Nova University Centre, SE-106 91, Stockholm, Sweden
[d] Idaho National Laboratory, Idaho Falls, ID, USA
[e] Australian Nuclear Science and Technology Organisation, Locked Bag 2001, Kirrawee DC, NSW 2232, Australia
[f] Westinghouse Electric Sweden, Västera SE-72163, Sweden
[g] Oak Ridge National Laboratory, 1 Bethel Valley Rd, Oak Ridge, TN 37831–6115, USA

ARTICLE INFO

Keywords:
A: Ceramic
B: Weight loss
C: Oxidation
C: High temperature corrosion
C: Kinetic parameters
C: Reactor conditions

ABSTRACT

The steam oxidation resistance of UN and UN-(20 vol%)ZrN fuel pellets is evaluated to enhance understanding of steam corrosion mechanisms in advanced nuclear fuel materials. In situ neutron diffraction shows the modified UN fuel pellets form a $(U_{0.77},Zr_{0.23})N$ solid-solution and the sole crystalline oxidation product detected in bulk is $(U_{0.77},Zr_{0.23})O_2$. U_2N_3 is not detected in significant quantities during the steam oxidation of UN or $(U_{0.77},Zr_{0.23})N$ and stable lattice parameters show that hydriding does not take place. Steam oxidation rates, obtained via sequential Rietveld refinement show how $(U_{0.77},Zr_{0.23})N$ has a higher activation energy (79 ± 1 kJmol^{-1} vs. 50 ± 5 kJmol^{-1}), higher onset temperature (430 °C vs. 400 °C) and slower reaction rates for steam oxidation up to 616 °C, than pure UN. Throughout, both UN and $(U_{0.77},Zr_{0.23})N$ exhibit linear (non-protective) oxidation kinetics, signifying that degradation of the fuel pellets is caused by the evolution of gaseous products at the interface followed by oxide scale spallation. This quantitative and mechanistic understanding of material degradation enables better defined operating regimes and points towards (U,Zr)N solid solutions as a promising strategy for the design of advanced nuclear fuel materials with enhanced steam corrosion resistance.

1. Introduction

To achieve the reduced carbon emissions outlined in the Paris Agreement, high-income countries need to increase their uptake of nuclear energy [1]. Adopters of nuclear technology are concerned about fuel safety margins, economics, and the generation of nuclear waste. Advanced nuclear fuels address these concerns by increasing the efficiency of energy generation and reducing the volume of spent fuel produced, without affecting safety margins [2].

Uranium mononitride (UN) is under consideration for use in next generation fast reactors and as drop-in UO_2 replacement for existing light water reactor (LWR) fuel assemblies [3,4]. The higher U density of 13.5 g.cm^{-3} in UN compared to 9.6 g.cm^{-3} for UO_2 fuel, enables UN to remain in the reactor for longer, producing less nuclear waste [5]. Attractive UN properties for fuel include high thermal conductivity, high melting temperature of ~ 2650 °C, and good fission product retention [6,7]. However, UN is highly reactive with water under normal LWR operating conditions, and is susceptible to oxidation and pulverisation in steam, under the high temperature conditions relevant for a fuel cladding breach [8,9].

The oxidation of uranium compounds typically follows a linear or parabolic rate law [10]. Linear kinetics are observed when the rate is limited by a surface reaction or diffusion through a gaseous phase. For a parabolic rate law, the material forms a protective barrier and oxidation is limited by diffusion through the oxide scale [11]. The formation of a protective oxide scale is beneficial to retard the oxidation rate of nuclear fuels, increasing the coping time in the event of an accident [12]. Several oxide-forming additives have been investigated to improve the corrosion resistance of uranium compounds. Suitable additives to improve the steam oxidation resistance of U_3Si_2 are limited by their relative thermodynamic stability of silicide formation [13]. For example, Mo, Mg, Ni, Ti and Zr cause dissociation of U_3Si_2 during synthesis, making them unsuitable dopants. Addition of Al to form $U_3Al_2Si_3$ and UAlSi delays the steam oxidation onset temperature of U_3Si_2 from 409 °C to > 800 °C

* Corresponding author at: School of Mechanical and Manufacturing Engineering, UNSW, Sydney, NSW 2033, Australia.
E-mail address: j.stansby@unsw.edu.au (J.H. Stansby).

https://doi.org/10.1016/j.corsci.2024.111877
Received 7 September 2023; Received in revised form 2 January 2024; Accepted 23 January 2024
Available online 26 January 2024
0010-938X/

[14]. However, since the U density in $U_3Al_2Si_3$ and UAlSi is lower than in UO_2, they are unlikely to be considered as prospective fuels by industry. U_3Si_2 alloyed with 2, 5.5, 7 and 10.3 vol% Cr increases the oxidation onset temperature of U_3Si_2 in steam to in region of 426 – 456 °C [14]. However, holding at 350 °C for 6 h pulverises the Cr-containing U_3Si_2 samples. U-Si-Y compositions, which are expected to form a protective Y_2O_3 layer, display no improvements in the steam oxidation behaviour [14].

UN-U_3Si_2 and UN-UO_2 composite materials have also been considered as next generation fuels. The corrosion resistance of UN in steam is improved by the addition of 10 wt% U_3Si_2, with SEM/EDS data shows that the U_3Si_2 phase preferentially reacts with oxygen over UN [9]. On the contrary, composite UN-(5–10 wt%)UO_2 pellets degrade more severely than UN in steam. [15] The difference is attributed to the occurrence of oxidation throughout the bulk of the pellet for the UN-UO_2 composite, as opposed to the reaction beginning at the surface and proceeding to the core for the pure UN pellet.

Using the sol gel and carbothermal reduction fabrication method, Herman *et al.* prepared UN pellets with 2.7 wt% Cr, 2.8 wt% Ni and 1.5 wt% Al, with improved corrosion properties in the Cr-doped pellet [16]. Cr-doped UN pellets manufactured by spark plasma sintering have a higher oxidation onset temperature in steam compared to UN, but a faster reaction rate once oxidation begins [17,18]. Due to their resistance to steam oxidation, Si, SiC, and ZrN were proposed as additives to improve the oxidation resistance of UN [5,19]. Preliminary results show that the addition of Si and SiC to UN leads to the formation of $USi_{1.67}$ and USi_3, respectively [19]. The high thermal conductivity, thermodynamic stability at high temperatures, low neutron absorption cross section, and full solubility between UN and ZrN makes ZrN a promising candidate for improving the oxidation properties of UN [20,21]. The addition of ZrN forms a single phase of UN with dissolved Zr, observed in peak shifts in XRD [5]. Malkki *et. al.* fabricated (U,Zr)N pellets containing 30 at% Zr. Boiling water autoclave tests showed that (U,Zr)N pellets start to disintegrate after 4 h at 150 °C, while pure UN pellets remain intact up to a temperature of 300 °C [22]. However, a mechanistic understanding of the steam corrosion of modified UN fuels is still lacking.

In particular, there is uncertainty in the literature regarding formation of an intermediate U_2N_3 phase. Formation of U_2N_3 upon hydrolysis of UN powder has been reported [23,24]. However, more recent steam oxidation studies on UN pellets do not observe any U_2N_3 [25,26]. Given the impact that intermediary species have on the thermochemistry of the oxidation process, neutronics and volume expansion of fuel pellets, it is important to determine whether U_2N_3 forms in significant quantities during the steam oxidation of UN fuel pellets.

Neutron diffraction enables quantitative phase and composition analysis of the bulk during the corrosion process – which are critical parameters because fuel stoichiometry and density directly impact reactor operation [27]. The amount of fissile U-235 must be known to obtain the fuel lifetime and effect on reactor control. In contrast to X-ray diffraction, for which scattering power scales with atomic number, neutron scattering length vary independently to the atomic number, Z. As such, neutron diffraction is well suited for the analysis of nuclear fuels in which high-Z elements, such as U, neighbour low-Z elements like N.

In situ neutron diffraction has been used to study the thermal expansion and oxidation in steam of U_3Si_2 and UN under transient conditions [25,28,29]. Such studies, which provide knowledge of a materials phase evolution and oxidation kinetics as a function of, for example, time and temperature, are needed to demonstrate the suitability of new nuclear fuels in existing and/or next generation reactor designs. Detailed knowledge and understanding of fuel performance under transient, accident-relevant conditions are necessary to licence a new commercial nuclear fuel such as $(U_{0.77},Zr_{0.23})N$ [30]. Specifically, the volume expansion of a fuel pellet is a key piece of information needed to design safe and long-lasting fuel bundles. The formation of hydride phases, best evaluated by neutron diffraction, leads to rapid and large volume expansion of the material and must be ruled out [18,29].

Herein, we evaluate the performance of UN-(20 vol%)ZrN and UN fuel pellets in high-temperature steam environments using in situ neutron diffraction, noting that the addition of non-uranium-containing components must be kept below 28 vol% to retain the advantageous uranium density of UN over UO_2 [5]. The neutron diffraction data demonstrates the beneficial effects of ZrN addition on the steam corrosion of UN. Through quantitative structural and phase analysis, the stoichiometry, volume expansion and steam oxidation mechanism of $(U_{0.77},Zr_{0.23})N$ is defined. The work also highlights the value of the in situ neutron diffraction method which enables the degradation mechanisms of nuclear materials in steam environments to be tracked fully, in real time.

2. Materials and methods

2.1. Sample fabrication

UN powder was synthesised from natural uranium metal (originally from the Institutt for Energiteknikk, Norway, carbon impurity level of 400 ppm.) by the hydriding-nitriding method, following the procedure and heating profile reported by Malkki *et al.* [31]. The resulting UN powder was transferred into an Ar-filled glovebox for handling. To yield the target composition of UN with 20 vol% ZrN, the UN powder (2.164 g) was mixed and ground in a mortar and pestle together with ZrN (0.268 g, Nanografi, 99.97%). The pure UN and modified UN-(20 vol%) ZrN powders which has the composition $(U_{0.77},Zr_{0.23})N$ were transferred into graphite sintering dies (9.3 mm inner diameter), lined on the inside with graphite paper. Sufficient powder to achieve a pellet height of approximately 3 mm was used. The resulting pellets were then spark plasma sintered (SPS) with a Dr. Sinter SPS 530-ET housed inside the Ar-filled glovebox. During the sintering procedure, the chamber was evacuated to a vacuum of 2 Pa and a constant uniaxial pressure of 45 MPa applied. Following an initial ramp at approximately 1.5 °C s^{-1}, the temperature was held at 1650 °C for 3 min.

The resulting microstructure and thermophysical properties of the pellets can be found in ref. [32]. The densities of the sintered pellets were measured by the Archimedes method in chloroform at 22 °C [6]. The oxygen concentrations were measured using the inert gas fusion technique with a Leco TC-136 analyser. Carbon concentrations were estimated from as-fabricated lattice parameter, via extrapolation of the data reported by Muromura *et al.* [33].

2.2. Neutron diffraction

In situ neutron diffraction data were collected on the high intensity neutron powder-diffractometer, Wombat [34]. The as-synthesised pellets were broken up into 3 smaller UN fragments and 2 smaller $(U_{0.77}, Zr_{0.23})N$ fragments and packed into a stainless-steel sample tube to enable the delivery of D_2O steam in a flow of He carrier gas. The tube assembly was placed inside an ILL-type high temperature vacuum furnace. The neutron wavelength (2.4131(3) Å), was determined using the NIST LaB_6 660b standard reference material [35]. Diffraction data were continuously collected every 60 s within $0.79 < Q < 4.81$ $Å^{-1}$. Gas flow of 85% He carrier gas and 15% D_2O steam (~70% humidity) was delivered using a Hiden Isochema XCS system, using a constant flow rate of 500 ml/min. This delivers 2.4–3.1 g/h of D_2O across the sample, a mass rate in excess by an order of magnitude compared to the fastest reaction rate measured in both experiments. The samples were first heated to 400 °C, 430 °C, 460 °C and 500 °C using a ramp rate of 10 °C min^{-1}, with an isothermal hold of approximately 5 h, 4 h, 2 h and 2 h at each temperature respectively. A ramp rate of 20 °C min^{-1} was applied to heat the samples to 680 °C, 700 °C, and 720 °C, where they were held for between 18 - 30 min at each temperature [18]. Finally, the heating system was turned off, and the samples were left cool to ~ 100 °C. The lower temperature (400 – 500 °C) and higher temperature (680 –

720 °C) regimes were chosen because preliminary steam oxidation tests indicate that there might be a change in rate and/or mechanism at 677 °C [18]. The increasingly shorter hold times at higher temperatures were chosen so that no more than 1/8 of the starting material oxidised at each isotherm. Multi-step heating is used to determine oxidation rates as a function of temperature. To determine activation energies, Arrhenius plots of $\ln k$ vs. $1/T$, where k is the oxidation rate (given in Table 4) and T is the sample temperature obtained using the stainless-steel lattice parameters, as described in the supporting information. Rearranging the Arrhenius equation to the form $y = mx + c$ to give $\ln k = \frac{-E_a}{RT} + \ln A$ enables the activation energies to be calculated from the slopes of the Arrhenius plots.

LAMP and GSAS-II software were used for neutron diffraction data reduction, visualization, and analysis. [36,37] Further details of the refinement methods are provided in the supporting information.

3. Results

Fig. 1 shows contour plots of the neutron diffraction data collected for UN and $(U_{0.77},Zr_{0.23})N$, together with the thermocouple temperature and D_2O flow rate, plotted as a function of time. Diffraction intensity (colour scale) is plotted against $Q = 4\pi\sin\theta/\lambda$ (horizonal axis). Successive diffraction patterns are stacked in time along the vertical axis. All reflections were accounted for by the starting material (UN or $(U_{0.77},Zr_{0.23})N$), the oxidation product (UO_2 or $(U_{0.77},Zr_{0.23})O_2$), or the sample holder (316 stainless-steel) Table 1.

Table 1
Sintering parameters, pellet density and impurity analysis for the UN, and $(U_{0.77},Zr_{0.23})N$ pellets.

Pellet	Pellet density, %	O_2 content / wt%	C content / wt%
UN	97	0.3	< 0.55
$(U_{0.77},Zr_{0.23})N$	99	0.4	< 0.55

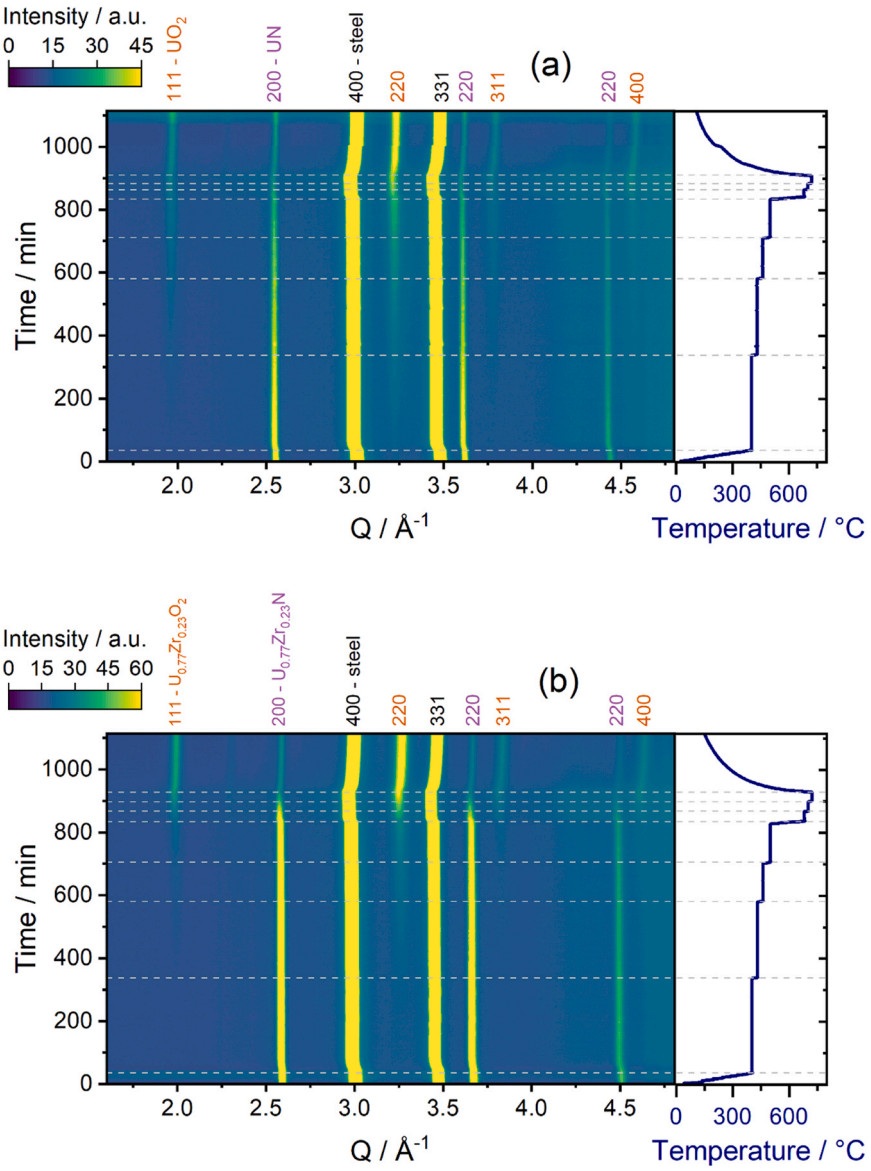

Fig. 1. Contour plots of in situ neutron diffraction data, together with the temperature profile for a) UN and b) $(U_{0.77},Zr_{0.23})N$. All visible peaks are accounted for by the 316 stainless-steel sample holder ($Fm\bar{3}m$) and a) UN ($Fm\bar{3}m$), UO_2 ($Fm\bar{3}m$), b) $(U_{0.77},Zr_{0.23})N$ ($Fm\bar{3}m$), $(U_{0.77},Zr_{0.23})O_2$ ($Fm\bar{3}m$). Grey dashed lines indicate isothermal holds at 400 °C, 430 °C, 460 °C, 500 °C, 680 °C, 700 °C, and 720 °C for a) 5 h, 4 h, 2 h, 2 h, 22 min, 18 min and 25 min and b) 5 h, 4 h, 2 h, 2 h, 30 min, 30 min and 30 min at each temperature respectively.

Table 2 details the phases present at the start and end of UN and $(U_{0.77},Zr_{0.23})N$ oxidation, as analysed by Rietveld refinement. At the start, there is an impurity of 1.9 wt% UO_2 in the UN sample while the UN-(20 vol%)ZrN sample is 100 wt% $(U_{0.77},Zr_{0.23})N$. No other phases are detected at the start of the experiment. On heating, there is some reversible reduction in peak intensity due to the Debye-Waller effect [38]. However, the non-reversible decrease in UN (or $(U_{0.77},Zr_{0.23})N$) peak intensity corresponds to the increase in UO_2 (or $(U_{0.77},Zr_{0.23})O_2$) peak intensity. This is visible in Fig. 1 and indicates an oxidation reaction. The reversible peak shift to lower Q (expansion) during heating and back to original position on cooling indicates lattice thermal expansion. The presence of UN and $(U_{0.77},Zr_{0.23})N$ diffraction peaks at the end of the experiments shows that some of the starting material remains unoxidised. The stainless-steel diffraction peaks are unchanging, except for thermal expansion shift.

Fig. 2, Table 3 and Table 4 show the Rietveld refinement results for UN and $(U_{0.77},Zr_{0.23})N$. The estimated standard deviations are given for the refined parameters. The lattice parameters of UN and $(U_{0.77},Zr_{0.23})N$ are 4.8956(1) Å and 4.8183(1) Å respectively, under ambient conditions.

The lattice strain points for UN and $(U_{0.77},Zr_{0.23})N$ as a function of temperature are shown in Fig. 3. No notable deviations from the thermal expansion line are observed throughout. The dependence of lattice constants on temperature, determined by the Rietveld refinement of neutron powder diffraction data, can be expressed by a quadratic equation of the form:

$$a = b_0 + b_1 T + b_2 T^2 \quad (1)$$

where b_0, b_1, and b_2 are constants and T is the temperature. Values of the constants were obtained by applying the least squares method to the lattice parameter data upon heating. The fitting results are given in Table 5.

Fig. 4 shows the UN and $(U_{0.77},Zr_{0.23})N$ relative wt. fraction (RWF) during isothermal holds, calculated as:

$$RWF = \frac{WF}{IWF} \times 100\% \quad (2)$$

where WF is the instantaneous wt. fraction of UN or $(U_{0.77},Zr_{0.23})N$ obtained from Rietveld refinement and *IWF* is the initial wt. fraction of UN or $(U_{0.77},Zr_{0.23})N$ available for oxidation at the start of the isothermal hold. Typical Rietveld refinement profiles during each isothermal hold are shown in Figs. S1 and S2.

The corrosion rates are constant for each isothermal hold, which is evidence of linear (i.e. non-protective) corrosion kinetics. [39] Table 6 details the oxidation rates at each isothermal hold, obtained by fitting the data shown in Fig. 4. For UN, oxidation is first detected during the 400 °C isothermal hold, at a rate of $0.497(5) \times 10^{-3}$ min^{-1}, and increases with temperature, reaching $8.2(6) \times 10^{-3}$ min^{-1} during the 680 °C isothermal hold. The rate of UN oxidation slows during the 700 °C and 720 °C isothermal holds to $4.6(7) \times 10^{-3}$ min^{-1} and $4.2(4) \times 10^{-3}$ min^{-1}, respectively. In contrast, oxidation of $(U_{0.77},Zr_{0.23})N$ begins during the 430 °C isothermal hold at a rate of $0.339(9) \times 10^{-3}$ min^{-1} and continues to increase with temperature to a maximum of $15.9(4) \times 10^{-3}$ min^{-1} during the 720 °C isothermal hold.

Arrhenius plots in Fig. 5 show a direct comparison of the corrosion rates between the two materials. The activation energies for steam oxidation of UN and $(U_{0.77},Zr_{0.23})N$ are 50 ± 5 kJmol^{-1} and 79 ± 1 kJmol^{-1}, respectively, as calculated from the slopes of the Arrhenius plots.

Table 2
Phases present at the start and end of the in situ corrosion experiments for the UN and UN-(20 vol%)ZrN fuel pellets.

Fuel pellet	Phases at start	Phases at end
UN	UN (98.1 ± 0.5 wt%)	UN (16.3 ± 2.2 wt%)
	UO_2 (1.9 ± 0.5 wt%)	UO_2 (83.7 ± 2.2 wt%)
UN-(20 vol%) ZrN	$(U_{0.77},Zr_{0.23})N$ (100 wt%)	$(U_{0.77},Zr_{0.23})N$ (13.0 ± 1.5 wt%)
		$(U_{0.77},Zr_{0.23})O_2$ (87.0 ± 1.5 wt%)

4. Discussion

Fig. 1 shows that bulk oxidation of $(U_{0.77},Zr_{0.23})N$ proceeds with the single oxidation product, $(U_{0.77},Zr_{0.23})O_2$, which has a lattice parameter of 5.419(2) Å, at 482 °C. The lattice parameter of $(U_{0.77},Zr_{0.23})N$ (4.8355 (1) Å) increases upon oxidation at 482 °C to $(U_{0.77},Zr_{0.23})O_2$ (5.419(2) Å), being 0.5835(2) Å (12%) larger. By comparison, the lattice parameter for UN (4.9154(3) Å) oxidised to UO_2 (5.4936(9) Å) at 482 °C increases by 0.5782(9) Å (also 12%). A 12% lattice parameter increase corresponds to a volumetric expansion of 41% for the oxidation of both UN and $(U_{0.77},Zr_{0.23})O_2$. The volumetric expansion obtained from in situ neutron diffraction is a key piece of information needed to design safe and long-lasting fuel bundles that can accommodate increased fuel volume without compromising the fuel cladding integrity.

Considering the findings discussed above, the oxidation of $(U_{0.77},Zr_{0.23})N$ in steam can be described by the following equations:

$$2\,(U_{0.77},Zr_{0.23})N + 4\,H_2O_{(g)} \rightarrow 2\,(U_{0.77},Zr_{0.23}O_2) + 2\,NH_{3\,(g)} + H_{2\,(g)} \quad (3)$$

$$2\,(U_{0.77},Zr_{0.23})N + 4\,H_2O_{(g)} \rightarrow 2\,(U_{0.77},Zr_{0.23}O_2) + N_{2\,(g)} + 4\,H_{2\,(g)} \quad (4)$$

The data in Fig. 4 shows that $(U_{0.77},Zr_{0.23})N$ has a higher oxidation onset temperature of 430 °C compared to 400 °C for UN but at higher temperatures $(U_{0.77},Zr_{0.23})N$ oxidises significantly faster. The point of intersection in Fig. 5 signifies that the temperature at which the rate of oxidation for $(U_{0.77},Zr_{0.23})N$ exceeds that of UN is 616 °C. In keeping with the higher oxidation onset temperature for $(U_{0.77},Zr_{0.23})N$, the activation energy for oxidation of $(U_{0.77},Zr_{0.23})N$ (79 ± 1 kJmol^{-1}) is higher than that of pure UN (50 ± 5 kJmol^{-1}). This detailed understanding of when oxidation begins and how the rates of oxidation changes as a function of temperature is key in defining the operating conditions in which next-generation, high uranium density, nuclear fuels can be used. The observed onset temperatures show how addition of Zr to UN will raise safe operating temperature to 430 °C, compared to 400 °C for pure UN. Moreover, the slower oxidation rates demonstrated for $(U_{0.77},Zr_{0.23})N$ shows that the addition of Zr increases the fuel safety margins, in the case of a cladding breach, if temperatures at the fuel-clad interface are kept below 616 °C.

A range of values have been reported for the steam oxidation onset of UN from < 200 °C for powders, 200 – 400 °C for monoliths, and > 600 °C for high purity, high density samples [26]. The onset temperature of 400 °C observed in this work, is typical for a UN fuel pellet. For comparison, oxidation onset temperatures for UO_2 are > 1000 °C, 405 – 480 °C for U_3Si_2, 629 °C for UB_2 and 400 °C for UC [40–44]. In addition to sample preparation, the method of determining the onset temperature, particularly if using differential thermal analysis (DTA) or thermogravimetric analysis (TGA), definition and the test conditions contribute to the variation in onset temperatures reported. As such, comparison between literature values from different labs should be treated with caution.

Elevated steam oxidation onset temperatures are often reported for composite materials. Combining U_3Si_2 with 10 wt% and 50 wt% UB_2 increases the onset temperature from 453 °C to 553 °C and 575 °C, respectively [43]. Additions of 5 wt% and 10 wt% Cr to U_3Si_2, which leads to the formation of a secondary U_2CrN_3 phase, causes the onset temperature to increase from 450 °C for monolithic U_3Si_2 to approximately 520 °C [45]. Here, we demonstrate that modified single-phase UN fuels can also display enhanced steam oxidation resistance.

The activation energy for steam oxidation of pure UN in this work (50 ± 5 kJmol^{-1}) is in good agreement with the value of 50.6 ± 1.3 kJmol^{-1} previously reported by Liu *et al.* [25] The lower activation energy for UN compared to that of 189.6 ± 29 kJmol^{-1} for polycrystalline UO_2 reflects the relatively poor steam oxidation behaviour of

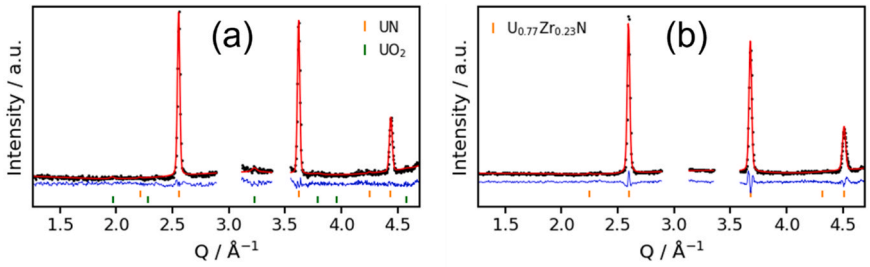

Fig. 2. Rietveld profiles for the first dataset collect for a) UN and b) $(U_{0.77},Zr_{0.23})O_2$. The observed data are shown as black dots, the calculated model in red, and difference between the observed and calculate model in blue. The vertical lines represent reflection markers for the indexed phases. Reflections arising from the sample holder have been excluded.

Table 3
Crystallographic parameters for UN as determined from Rietveld analysis of NPD data.

Atom	Site	x	y	z	SOF	$U_{iso} \times 100$ / Å^2
U	4*a*	0	0	0	1	1.8(3)
N	4*b*	0.5	0.5	0.5	1	1.2(2)

Space group $Fm\bar{3}m$, weighted profile R-factor wR_p = 2.6%, a = 4.8956(1) Å. SOF = Site occupancy factor.

Table 4
Crystallographic parameters for $(U_{0.77},Zr_{0.23})N$ as determined from Rietveld analysis of NPD data.

Atom	Site	x	y	z	SOF	$U_{iso} \times 100$ / Å^2
U	4*a*	0	0	0	0.77(4)*	1.6(3)
Zr	4a	0	0	0	0.23(4)*	1.6(3)
N	4*b*	0.5	0.5	0.5	1	2.0(3)

Space group $Fm\bar{3}m$, weighted profile R-factor wR_p = 3.1%, a = 4.8183(1) Å. SOF = site occupancy factor. *Sum constrained to 1.

UN [46]. Comparable activation energies to that of UN have been reported for U-metal foil (46.9 ± 1.3 kJmol^{-1}, below 350 °C) and U-metal bar stock (58.0 ± 3.8 kJmol^{-1}, below 300 °C), the difference being that at higher temperatures the oxide layer adheres to the underlying U-metal forming a protective surface layer [47]. Activation energy values for the steam oxidation of alternative next generation fuels such as U_3Si_2, UC and UB_2 are lacking. However, air oxidation studies indicate that U_3Si_2 is most prone to oxidation followed by UC, UN, UO_2 and UB_2, with reported values of 36 - 90 kJmol^{-1} (depending on the U_3Si_2 microstructure), 120 kJmol^{-1}, 124 kJmol^{-1}, 154 kJmol^{-1} and 380 kJmol^{-1} (for temperatures below 600 °C and 25 kJmol^{-1} above), respectively [48–52]. For both $(U_{0.77},Zr_{0.23})N$ and UN, linear corrosion rates (i.e. non-protective oxide formation) are observed throughout and no change in oxidation mechanism is observed. There is no evidence of logarithmic, parabolic or sub-parabolic regimes which would signify formation of a protective oxide. Instead, the linear corrosion rates also indicates that steam oxidation of $(U_{0.77},Zr_{0.23})N$ and UN is limited by either a surface reaction (adsorption / chemisorption) or diffusion through the gas phase. This can occur when i) the oxide scale is porous and/or discontinuous or when ii) compressive stress in the oxide scale causes spallation and cracking, continually exposing a fresh surface [39]. The steam oxidation of nitrides generates gaseous products (e.g. NH_3, N_2). N_2 and H_2 are evolved during the reaction of ZrN with steam and it has been suggested that pores and cracks may be caused by bubbles containing gaseous reaction products [53]. Steam oxidation of UN and $(U_{0.77},Zr_{0.23})N$ generates NH_3, N_2 and H_2. Our results indicate that formation of gases at the interface of $(U_{0.77},Zr_{0.23})N$ and UN leads to spallation of the oxide scale and thus mechanical failure of the fuel pellets. Comparable rate limiting steps have been observed during the corrosion of Fe, Co and Ti alloys [54,55]. Moreover, ex situ SEM images of UN post steam oxidation show the UO_2 scale separating from the bulk sample, as expected upon oxide spallation [18].

A reduction in oxidation rate is observed for UN during the 700 and 720 °C isothermal holds, see Figs. 4 and 5. Given that there is no change in the oxidation mechanism, it is possible that the accumulation of porous/cracked oxide limits the flow of D_2O over the sample. Changes in the surface morphology throughout the experiment, particularly at the higher isothermal holds where the pellets contained a lower portion of

Table 5
Dependence of lattice parameters as a function of temperature, expressed as a quadratic. # Root mean square percentage error, % (RMSPE).

Composition	Equation	RMSPE#
UN	$a = 4.8940(1) + 4.62(4) \times 10^{-5}T + 8(1)\times10^{-9}T^2$	0.044
$(U_{0.77},Zr_{0.23})N$	$a = 4.8157(1) + 3.46(4) \times 10^{-5}T + 1.45(4)\times10^{-8}T^2$	0.039

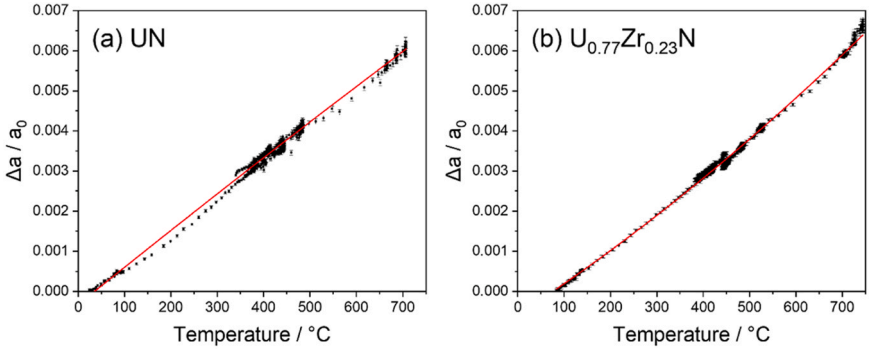

Fig. 3. Lattice strain as a function of temperature upon heating for a) UN and b) $(U_{0.77},Zr_{0.23})N$.

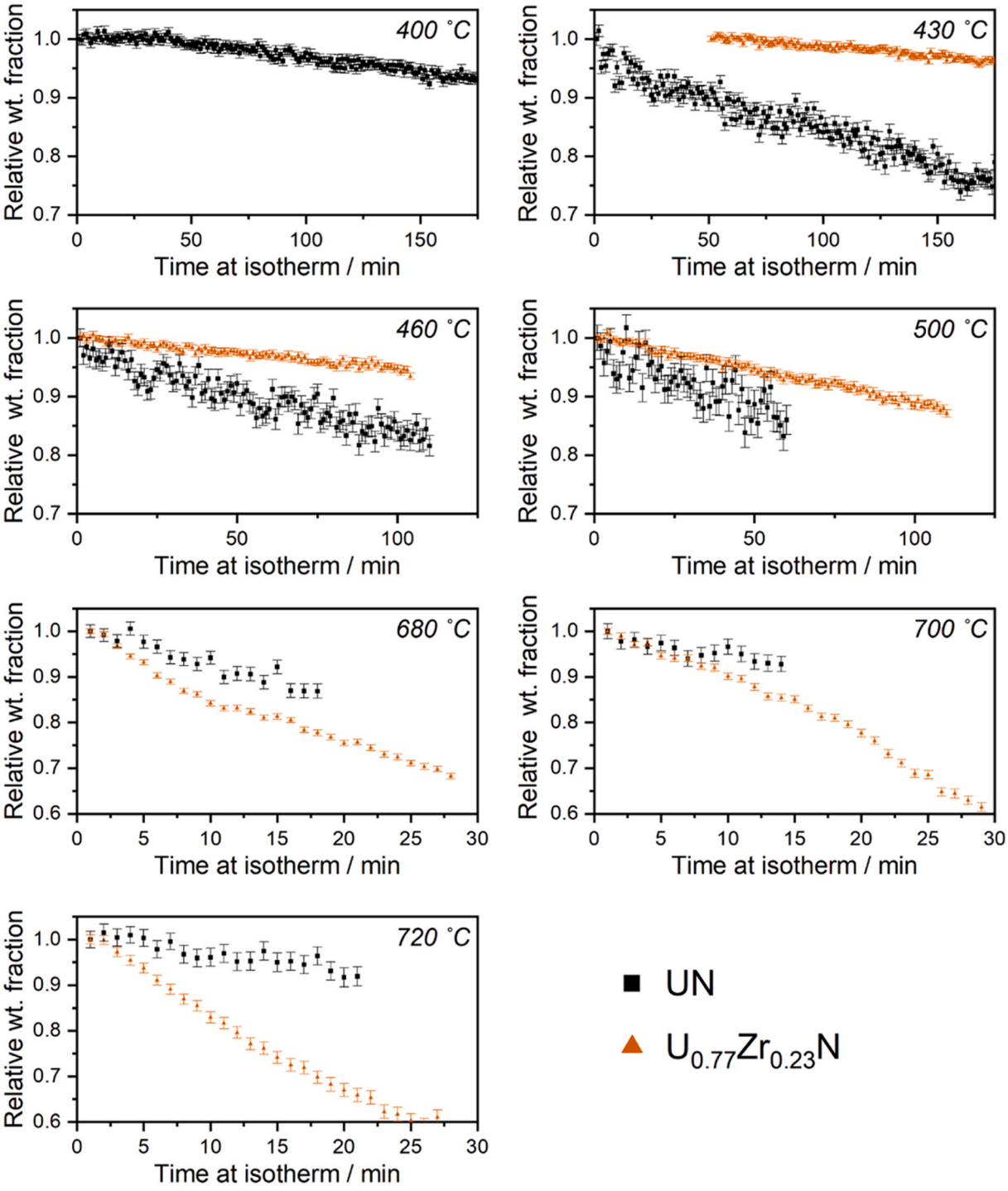

Fig. 4. RWF of UN and $(U_{0.77},Zr_{0.23})N$ as a function of time during isothermal holds.

Table 6
Oxidation rates (x 10^{-3} / min^{-1}) for the UN and $(U_{0.77},Zr_{0.23})N$ fuel pellets.

Isotherm / °C	400	430	460	500	680	700	720
UN	-0.497(5)	-1.19(2)	-1.36(5)	-2.0(2)	-8.2(6)	-4.6(7)	-4.2(4)
$(U_{0.77},Zr_{0.23})N$	n/a	-0.339(9)	-0.536(13)	-1.14(1)	-10.9(4)	-13.8(4)	-15.9(4)

nitride fuel may also contribute to the slower rates for UN. It is also hypothesised that above 616 °C the $(U_{0.77},Zr_{0.23})O_2$ scale breaks down more easily than UO_2, giving rise to the higher oxidation rate observed for $(U_{0.77},Zr_{0.23})N$ at elevated temperatures. However, further work is needed to understand why the presence of Zr increases the oxidation rate of UN at temperatures above 616 °C.

Fig. 3 shows that no significant peak shifts are observed during the isothermal periods, indicating no hydriding of $(U_{0.77},Zr_{0.23})N$ or UN,

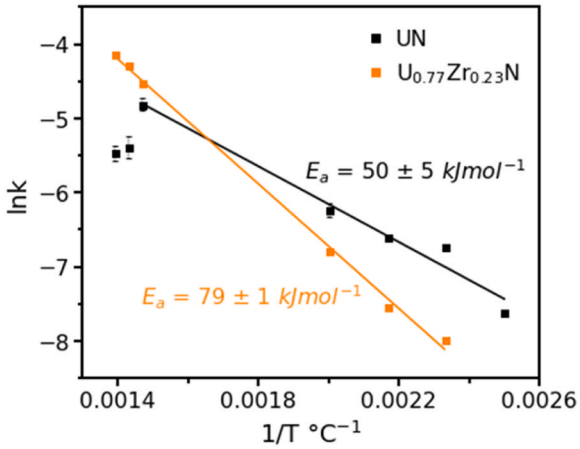

Fig. 5. Arrhenius plots for the oxidation of UN and $(U_{0.77},Zr_{0.23})N$ in steam. Where not visible, error bars are smaller than the symbol.

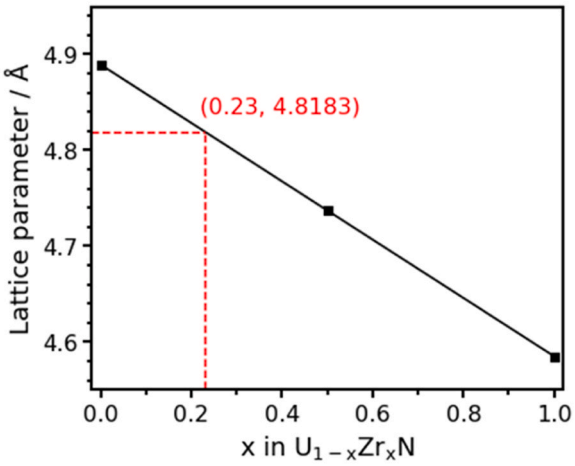

Fig. 6. Change in lattice parameter as a function of x in $U_{1-x}Zr_xN$. Plotted values (square markers) are obtained from the literature [59–61]. Linear interpolation (solid line), according to Vegard's law, shows that the measured lattice parameter of a = 4.8183 Å (see also Fig. 2 and Table 4) corresponds to the composition $(U_{0.77},Zr_{0.23})N$.

unlike reported for U_3Si_2 [29]. The rapid thermal expansion that accompanies hydriding can create sufficient stress to unzip the breached cladding in a LWR accident scenario [56]. Here, we show that hydriding of $(U_{0.77},Zr_{0.23})N$ or UN is not a concern upon exposure to steam. Moreover, the smaller thermal expansion of $(U_{0.77},Zr_{0.23})N$ is beneficial for minimising pellet-cladding mechanical interaction during operation which can limit the lifetime of the fuel in reactors [57].

No $U_{2-x}Zr_xN_3$ or U_2N_3 is detected throughout the steam oxidation of $(U_{0.77},Zr_{0.23})N$ or UN, respectively. Some previous works have reported the formation of U_2N_3 as well as UO_2 upon hydrolysis of UN powder [23,24]. However, our results, which are more representative of the bulk material, support more recent steam oxidation studies on UN pellets for which no U_2N_3 is observed [25,26]. The formation of U_2N_3 (or lack of) plays an important role in the thermochemistry of the oxidation process and impacts the volume expansion of monolithic samples [5]. The present study shows that $U_{2-x}Zr_xN_3$ or U_2N_3 do not form in significant quantities of the bulk material and need not be considered in the macro steam corrosion mechanism of $(U_{0.77},Zr_{0.23})N$ and UN.

The single set of shifted diffraction peaks in the $(U_{0.77},Zr_{0.23})N$ neutron data (Fig. S2) indicates a solid solution between UN and ZrN as a single-phase. The lattice parameter of the $(U_{0.77},Zr_{0.23})N$ phase, 4.8183 (1) Å, is ~ 1.6% (0.0773 Å) smaller than that of pure UN, driven by the smaller atomic radius of Zr compared with U [58]. The refined U and Zr site occupancy factors indicate a stoichiometry of $U_{0.77(4)}Zr_{0.23(4)}N$. Site occupancy calculated using Vegard's law (Fig. 6), and the $(U_{0.77},Zr_{0.23})N$ lattice parameter of 4.8183(1) Å yields a value of x = 0.23(1), in close agreement, meaning we can confidently assign the stoichiometry of the uranium nitride fuel pellet with enhance corrosion resistance to be $(U_{0.77},Zr_{0.23})N$. As such, the work highlights the formation of single-phase solid solutions with UN as a pathway to achieving enhanced corrosion resistance in high density nuclear fuels.

Given that the addition of Zr to UN diminishes the advantages of UN over the benchmark UO_2 in terms of uranium density, future studies should investigate the corrosion behaviour of $(U_{1-x},Zr_x)N$ as a function of decreasing Zr content.

5. Conclusions

In situ neutron diffraction experiments show that 20 vol% additions of ZrN to UN increases the oxidation onset temperature in steam from 400 °C to 430 °C and results in a higher activation barrier for oxidation of 79 ± 1 kJmol^{-1}, vs 50 ± 5 kJmol^{-1}. Compared with UN, $(U_{0.77},Zr_{0.23})N$ displays slower oxidation rates at temperatures up to 616 °C, but faster rates above this temperature. In addition to observing quantitative rate equations, two possible mechanisms are identified for the oxidation of $(U_{0.77},Zr_{0.23})N$, yielding $(U_{0.77},Zr_{0.23})O_2$, H_2 and either NH_3 or N_2. Both UN and $(U_{0.77},Zr_{0.23})N$ exhibit linear (non-protective) oxidation kinetics throughout, signifying that mechanical failure of the fuel pellets is caused by the evolution of gaseous products at the interface and the ensuing spallation of UO_2 and $(U_{0.77},Zr_{0.23})O_2$ oxidation products. We show that U_2N_3, which plays an important role in the thermochemistry and mechanics of the oxidation process, does not form in significant quantities during the steam oxidation of UN or $(U_{0.77},Zr_{0.23})N$. Stable lattice parameters in high temperature steam show that hydriding of $(U_{0.77},Zr_{0.23})N$ or UN is not a concern upon exposure to steam. The enhanced performance of $(U_{0.77},Zr_{0.23})N$ in high temperature steam, observed by in situ neutron diffraction, points towards single-phase UN solid solutions as a promising pathway to achieving enhanced corrosion resistance in nuclear fuels for next generation reactors.

CRediT authorship contribution statement

Stansby Jennifer Helen: Formal analysis, Investigation, Writing – original draft. **Mischenko Yulia:** Investigation, Writing – review & editing. **Patnaik Sobhan:** Investigation. **Peterson Vanessa K:** Methodology, Writing – review & editing. **Baldwin Christopher:** Methodology. **Burr Patrick A:** Supervision, Writing – review & editing. **Adorno-Lopes Denise:** Conceptualization, Resources, Supervision, Writing – review & editing. **Obbard Edward G:** Conceptualization, Funding acquisition, Investigation, Writing – review & editing.

Declaration of Competing Interest

The authors declare that they have no known competing financial interests or personal relationships that could have appeared to influence the work reported in this paper.

Data availability

Data will be made available on request.

Acknowledgements

The authors acknowledge funding for beamtime proposal P9782 at the Australian Centre for Neutron Scattering (ACNS). JHS, EGO and PAB acknowledge funding from ANSTO and the Sir William Tyree Foundation. The authors are also grateful for the assistance of John MacLeod,

Richard Collins, Deborah Wakeham, Daniel Gregg and Grant Griffiths in making the experiments possible.

Appendix A. Supporting information

Supplementary data associated with this article can be found in the online version at doi:10.1016/j.corsci.2024.111877.

References

[1] Nuclear technology's role in the world's energy supply is shrinking, Nature, 591, 2021. pp. 177–178.https://doi.org/10.1038/d41586–021-00615-w.

[2] F. Cappia, K. Wright, D. Frazer, K. Bawane, B. Kombaiah, W. Williams, S. Finkeldei, F. Teng, J. Giglio, M.N. Cinbiz, B. Hilton, J. Strumpell, R. Daum, K. Yueh, C. Jensen, D. Wachs, Detailed characterization of a PWR fuel rod at high burnup in support of LOCA testing, J. Nucl. Mater. 569 (2022) 153881, https://doi.org/10.1016/j.jnucmat.2022.153881.

[3] V.G. Goncharov, J. Liu, A. van Veelen, K. Kriegsman, C. Benmore, C. Sun, S. Kelly, J.T. White, H. Xu, X. Guo, Energetics of oxidation and formation of uranium mononitride, J. Nucl. Mater. 569 (2022) 153904, https://doi.org/10.1016/j.jnucmat.2022.153904.

[4] S.J. Zinkle, K.A. Terrani, J.C. Gehin, L.J. Ott, L.L. Snead, Accident tolerant fuels for LWRs: a perspective, J. Nucl. Mater. 448 (2014) 374–379, https://doi.org/10.1016/j.jnucmat.2013.12.005.

[5] J.K. Watkins, A. Gonzales, A.R. Wagner, E.S. Sooby, B.J. Jaques, Challenges and opportunities to alloyed and composite fuel architectures to mitigate high uranium density fuel oxidation: uranium mononitride, J. Nucl. Mater. 553 (2021) 153048, https://doi.org/10.1016/j.jnucmat.2021.153048.

[6] Y. Mishchenko, K.D. Johnson, J. Wallenius, D.A. Lopes, Design and fabrication of UN composites: from first principles to pellet production, J. Nucl. Mater. 553 (2021) 153047, https://doi.org/10.1016/j.jnucmat.2021.153047.

[7] D.M. King, S.T. Liddle, Progress in molecular uranium-nitride chemistry, Coord. Chem. Rev. 266-267 (2014) 2–15, https://doi.org/10.1016/j.ccr.2013.06.013.

[8] E. Lawrence Bright, S. Rennie, A. Siberry, K. Samani, K. Clarke, D.T. Goddard, R. Springell, Comparing the corrosion of uranium nitride and uranium dioxide surfaces with H_2O_2, J. Nucl. Mater. 518 (2019) 202–207, https://doi.org/10.1016/j.jnucmat.2019.03.006.

[9] D.A. Lopes, S. Uygur, K. Johnson, Degradation of UN and UN–U_3Si_2 pellets in steam environment, J. Nucl. Sci. Technol. 54 (2017) 405–413, https://doi.org/10.1080/00223131.2016.1274689.

[10] D. Cubicciotti, The reaction between uranium and oxygen, J. Am. Chem. Soc. 74 (1952) 1079–1081, https://doi.org/10.1021/ja01124a505.

[11] D.J. Young, High Temperature Oxidation and Corrosion of Metals, Elsevier,, 2008.

[12] C. Parisi, Z. Ma, D. Mandelli, N. Anderson, H. Zhang, Risk-informed safety analysis for accident tolerant fuels, Nucl. Sci. Eng. 194 (2020) 748–770, https://doi.org/10.1080/00295639.2020.1732699.

[13] A. Gonzales, J.K. Watkins, A.R. Wagner, B.J. Jaques, E.S. Sooby, Challenges and opportunities to alloyed and composite fuel architectures to mitigate high uranium density fuel oxidation: uranium silicide, J. Nucl. Mater. 553 (2021) 153026, https://doi.org/10.1016/j.jnucmat.2021.153026.

[14] E.S. Wood, C. Moczygemba, G. Robles, Z. Acosta, B.A. Brigham, C.J. Grote, K. E. Metzger, L. Cai, High temperature steam oxidation dynamics of U_3Si_2 with alloying additions: Al, Cr, and Y, J. Nucl. Mater. 533 (2020) 152072, https://doi.org/10.1016/j.jnucmat.2020.152072.

[15] J.K. Watkins, D.P. Butt, B.J. Jaques, Microstructural degradation of UN and UN-UO_2 composites in hydrothermal oxidation conditions, J. Nucl. Mater. 518 (2019) 30–40, https://doi.org/10.1016/j.jnucmat.2019.02.027.

[16] A. Herman, C. Ekberg, A uranium nitride doped with chromium, nickel or aluminum as an accident tolerant fuel, Res. Rev.: J. Mater. Sci. 05 (2017) 83–99, https://doi.org/10.4172/2321-6212.1000196.

[17] K. Yang, E. Kardoulaki, D. Zhao, B. Gong, A. Broussard, K. Metzger, J.T. White, M. R. Sivack, K.J. McClellan, E.J. Lahoda, J. Lian, Cr-incorporated uranium nitride composite fuels with enhanced mechanical performance and oxidation resistance, J. Nucl. Mater. 559 (2022) 153486, https://doi.org/10.1016/j.jnucmat.2021.153486.

[18] Y. Mishchenko, K.D. Johnson, D. Jädernäs, J. Wallenius, D.A. Lopes, Uranium nitride advanced fuel: an evaluation of the oxidation resistance of coated and doped grains, J. Nucl. Mater. 556 (2021) 153249, https://doi.org/10.1016/j.jnucmat.2021.153249.

[19] A.P. Shivprasad, A.C. Telles, J.T. White, Report on waterproofing of UN studies, in, Los Alamos National Lab.(LANL), Los Alamos, NM (United States), 2019.

[20] M. Burghartz, G. Ledergerber, H. Hein, R.R. van der Laan, R.J.M. Konings, Some aspects of the use of ZrN as an inert matrix for actinide fuels, J. Nucl. Mater. 288 (2001) 233–236, https://doi.org/10.1016/S0022-3115(00)00722-4.

[21] M. Pukari, O. Runevall, N. Sandberg, J. Wallenius, Vacancy formation and solid solubility in the U–Zr–N system, J. Nucl. Mater. 406 (2010) 351–355, https://doi.org/10.1016/j.jnucmat.2010.09.006.

[22] P. Malkki, The manufacturing of uranium nitride for possible use in light water reactors, in, KTH Royal Institute of Technology, 2015.

[23] R.M. Dell, V.J. Wheeler, N.J. Bridger, Hydrolysis of uranium mononitride, Trans. Faraday Soc. 63 (1967) 1286–1294, https://doi.org/10.1039/TF9676301286.

[24] S. Sugihara, S. Imoto, Hydrolysis of uranium nitrides, J. Nucl. Sci. Technol. 6 (1969) 237–242, https://doi.org/10.1080/18811248.1969.9732878.

[25] J. Liu, C. Gasparrini, J.T. White, K. Johnson, D.A. Lopes, V.K. Peterson, A. Studer, G.J. Griffiths, G.R. Lumpkin, M.R. Wenman, P.A. Burr, E.S. Sooby, E.G. Obbard, Thermal expansion and steam oxidation of uranium mononitride analysed via in situ neutron diffraction, J. Nucl. Mater. 575 (2023) 154215, https://doi.org/10.1016/j.jnucmat.2022.154215.

[26] E.S. Sooby, B.A. Brigham, G. Robles, J.T. White, S.W. Paisner, E. Kardoulaki, B. Williams, Steam oxidation of uranium mononitride in pure and reducing steam atmospheres to 1200 °C, J. Nucl. Mater. 560 (2022) 153487, https://doi.org/10.1016/j.jnucmat.2021.153487.

[27] T.L. Ulrich, S.C. Vogel, J.T. White, D.A. Andersson, E.S. Wood, T.M. Besmann, High temperature neutron diffraction investigation of U_3Si_2, Materialia 9 (2020) 100580, https://doi.org/10.1016/j.mtla.2019.100580.

[28] E.G. Obbard, K.D. Johnson, P.A. Burr, D.A. Lopes, D.J. Gregg, K.D. Liss, G. Griffiths, N. Scales, S.C. Middleburgh, Anisotropy in the thermal expansion of uranium silicide measured by neutron diffraction, J. Nucl. Mater. 508 (2018) 516–520, https://doi.org/10.1016/j.jnucmat.2018.04.049.

[29] J. Liu, P.A. Burr, J.T. White, V.K. Peterson, P. Dayal, C. Baldwin, D. Wakeham, D. J. Gregg, E.S. Sooby, E.G. Obbard, Structural and phase evolution in U_3Si_2 during steam corrosion, Corros. Sci. 204 (2022) 110373, https://doi.org/10.1016/j.corsci.2022.110373.

[30] D.A. Andersson, X.Y. Liu, B. Beeler, S.C. Middleburgh, A. Claisse, C.R. Stanek, Density functional theory calculations of self- and Xe diffusion in U3Si2, J. Nucl. Mater. 515 (2019) 312–325, https://doi.org/10.1016/j.jnucmat.2018.12.021.

[31] P. Malkki, M. Jolkkonen, T. Hollmer, J. Wallenius, Manufacture of fully dense uranium nitride pellets using hydride derived powders with spark plasma sintering, J. Nucl. Mater. 452 (2014) 548–551, https://doi.org/10.1016/j.jnucmat.2014.06.012.

[32] Y. Mishchenko, S. Patnaik, J. Wallenius, D.A. Lopes, Thermophysical properties and oxidation behaviour of the $U_{0.8}Zr_{0.2}N$ solid solution, Nucl. Mater. Energy (2023) (under review).

[33] T. Muromura, H. Tagawa, Lattice parameter of uranium mononitride, J. Nucl. Mater. 79 (1979) 264–266, https://doi.org/10.1016/0022-3115(79)90457-4.

[34] A.J. Studer, M.E. Hagen, T.J. Noakes, Wombat: The high-intensity powder diffractometer at the OPAL reactor, Phys. B: Condens. Matter 385-386 (2006) 1013–1015, https://doi.org/10.1016/j.physb.2006.05.323.

[35] D.R. Black, D. Windover, A. Henins, J. Filliben, J.P. Cline, Certification of standard reference material 660B, Powder Diffr. 26 (2011) 155–158, https://doi.org/10.1154/1.3591064.

[36] D. Richard, M. Ferrand, G.J. Kearley, Analysis and visualisation of neutron-scattering data, J. Neutron Res. 4 (1996) 33–39, https://doi.org/10.1080/10238169608200065.

[37] B.H. Toby, R.B. Von Dreele, GSAS-II: the genesis of a modern open-source all purpose crystallography software package, J. Appl. Crystallogr. 46 (2013) 544–549, https://doi.org/10.1107/S0021889813003531.

[38] B.E. Warren, X-ray Diffraction, Courier Corporation, 1990.

[39] E. McCafferty, Introduction to Corrosion Science, Springer Science & Business Media,, 2010.

[40] E.S. Wood, J.T. White, C.J. Grote, A.T. Nelson, U_3Si_2 behavior in H_2O: part I, flowing steam and the effect of hydrogen, J. Nucl. Mater. 501 (2018) 404–412, https://doi.org/10.1016/j.jnucmat.2018.01.002.

[41] C. Moczygemba, J. George, E. Montoya, E. Kim, G. Robles, E. Sooby, Structure characterization and steam oxidation performance of U_3Si_2 with Zr alloying additions, J. Nucl. Mater. 570 (2022) 153951, https://doi.org/10.1016/j.jnucmat.2022.153951.

[42] J.H. Yang, D.S. Kim, D.-J. Kim, S. Kim, J.-H. Yoon, H.S. Lee, Y.-H. Koo, K.W. Song, Oxidation and phase separation of U_3Si_2 nuclear fuel in high-temperature steam environments, J. Nucl. Mater. 542 (2020) 152517, https://doi.org/10.1016/j.jnucmat.2020.152517.

[43] J. Turner, T. Abram, Steam performance of UB_2/U_3Si_2 composite fuel pellets, compared to U_3Si_2 reference behaviour, J. Nucl. Mater. 529 (2020) 151919, https://doi.org/10.1016/j.jnucmat.2019.151919.

[44] C.P. Kempter, Hydrolysis properties of uranium monocarbide and dicarbide, J. Less Common Met. 4 (1962) 419–425, https://doi.org/10.1016/0022-5088(62)90026-7.

[45] B. Gong, L. Cai, P. Lei, K.E. Metzger, E.J. Lahoda, F.A. Boylan, K. Yang, J. Fay, J. Harp, J. Lian, Cr-doped U_3Si_2 composite fuels under steam corrosion, Corros. Sci. 177 (2020) 109001, https://doi.org/10.1016/j.corsci.2020.109001.

[46] J. Abrefah, A. de Aguiar Braid, W. Wang, Y. Khalil, D. Olander, High temperature oxidation of UO2 in steam-hydrogen mixtures, J. Nucl. Mater. 208 (1994) 98–110.

[47] P.J. Hayward, D.G. Evans, P. Taylor, I.M. George, A.M. Duclos, Oxidation of uranium in steam, J. Nucl. Mater. 217 (1994) 82–92, https://doi.org/10.1016/0022-3115(94)90307-7.

[48] R. Worth, D. Goddard, J. Buckley, R. Harrison, H. Liu, J. Paul, T. Abram, Oxidation of U_3Si_2: the role of exothermic energy, J. Nucl. Mater. 568 (2022) 153874.

[49] B. Gong, K. Yang, D. Zhao, A.T. Nelson, J. Lian, Oxidation kinetics of SPS-densified U_3Si_2 fuels—microstructure impact, J. Appl. Phys. 131 (2022).

[50] T. Ohmichi, T. Honda, The oxidation of UC and UN powder in Air, J. Nucl. Sci. Technol. 5 (1968) 600–602, https://doi.org/10.1080/18811248.1968.9732521.

[51] R.J. McEachern, P. Taylor, A review of the oxidation of uranium dioxide at temperatures below 400C, J. Nucl. Mater. 254 (1998) 87–121.

[52] Q. Mistarihi, F. Martini, J. Buckley, S.C. Middleburgh, T.J. Abram, J. Turner, The oxidation of uranium diboride in flowing air atmospheres, J. Nucl. Mater. 580 (2023) 154417, https://doi.org/10.1016/j.jnucmat.2023.154417.

[53] Z. Gao, Y. Chen, J. Kulczyk-Malecka, P. Kelly, Y. Zeng, X. Zhang, C. Li, H. Liu, N. Rohbeck, P. Xiao, Comparison of the oxidation behavior of a zirconium nitride

coating in water vapor and air at high temperature, Corros. Sci. 138 (2018) 242–251, https://doi.org/10.1016/j.corsci.2018.04.015.
[54] I. Chattoraj, Stress Corrosion Cracking (SCC) and Hydrogen-assisted Cracking in Titanium Alloys, Woodhead Publishing, 2011.
[55] L. Rosenblum, Mechanism and Kinetics of Corrosion of Selected Iron and Cobalt Alloys in Refluxing Mercury, National Aeronautics and Space Administration, 1968.
[56] R.T. Sweet, Y. Yang, K.A. Terrani, B.D. Wirth, A.T. Nelson, Performance of U_3Si_2 in an LWR following a cladding breach during normal operation, J. Nucl. Mater. 539 (2020) 152263, https://doi.org/10.1016/j.jnucmat.2020.152263.
[57] Y. Yun, Thermal expansion, in, No. NEA-NSC-R–2015–5. 2015, pp. 177.
[58] R. Shannon, Revised effective ionic radii and systematic studies of interatomic distances in halides and chalcogenides, Acta Crystallogr. Sect. A 32 (1976) 751–767, https://doi.org/10.1107/S0567739476001551.
[59] R.E. Rundle, N.C. Baenziger, A.S. Wilson, R.A. McDonald, The structures of the carbides, nitrides and oxides of uranium, J. Am. Chem. Soc. 70 (1948) 99–105, https://doi.org/10.1021/ja01181a029.
[60] A.N. Christensen, A neutron diffraction investigation on single crystals of titanium carbide, titanium nitride, and zirconium nitride, Acta Chem. Scand. 29 (1975) 563–568, https://doi.org/10.3891/acta.chem.scand.29a-0563.
[61] C. Kouhsen, A. Naoumidis, H. Nickel, Preparation and thermochemical stability of uranium-zirconium-carbonitrides, J. Nucl. Mater. 61 (1976) 88–98, https://doi.org/10.1016/0022-3115(76)90101-X.